




Article

Efficacy of Prednisolone/Zn Metal Complex and Artemisinin Either Alone or in Combination on Lung Functions after Excessive Exposure to Electronic Cigarettes Aerosol with Assessment of Antibacterial Activity

Reham Z. Hamza ^{1,*}, Fatima S. Alaryani ², Reem E. Alotaibi ¹, Maha A. Al-Harathi ¹, Ghadeer S. Alotaibi ¹, Nora A. Al-Subaie ¹, Amjad A. Al-Talhi ¹, Bander Al-Bogami ¹, Najah M. Al-Baqami ³, Samy M. El-Megharbel ⁴ and Eman H. Al-Thubaiti ⁵

¹ Biology Department, Main Campus, College of Sciences, Taif University, Taif 21944, Saudi Arabia; s43903047@students.tu.edu.sa (R.E.A.); s43902557@students.tu.edu.sa (M.A.A.-H.); s43900899@students.tu.edu.sa (G.S.A.); s4301260@students.tu.edu.sa (N.A.A.-S.); s43901735@students.tu.edu.sa (A.A.A.-T.); b.boqami@tu.edu.sa (B.A.-B.)

² Department of Biology, College of Science, University of Jeddah, Jeddah 21589, Saudi Arabia; fsalaryani@uj.edu.sa

³ Department of Biological Sciences, Zoology, Faculty of Science, King Abdul-Aziz University, Jeddah 21589, Saudi Arabia; nalbogami@kau.edu.sa

⁴ Chemistry Department, Main Campus, College of Sciences, Taif University, Taif 21944, Saudi Arabia; s.megherbel@tu.edu.sa

⁵ Biotechnology Department, Main Campus, College of Sciences, Taif University, Taif 21944, Saudi Arabia; i.althubaiti@tu.edu.sa

* Correspondence: reham.z@tu.edu.sa



Citation: Hamza, R.Z.; Alaryani, F.S.; Alotaibi, R.E.; Al-Harathi, M.A.; Alotaibi, G.S.; Al-Subaie, N.A.; Al-Talhi, A.A.; Al-Bogami, B.; Al-Baqami, N.M.; El-Megharbel, S.M.; et al. Efficacy of Prednisolone/Zn Metal Complex and Artemisinin Either Alone or in Combination on Lung Functions after Excessive Exposure to Electronic Cigarettes Aerosol with Assessment of Antibacterial Activity. *Crystals* **2022**, *12*, 972. <https://doi.org/10.3390/cryst12070972>

Academic Editor: Marian Valko

Received: 14 May 2022

Accepted: 5 July 2022

Published: 12 July 2022

Publisher's Note: MDPI stays neutral with regard to jurisdictional claims in published maps and institutional affiliations.



Copyright: © 2022 by the authors. Licensee MDPI, Basel, Switzerland. This article is an open access article distributed under the terms and conditions of the Creative Commons Attribution (CC BY) license (<https://creativecommons.org/licenses/by/4.0/>).

Abstract: The use of transition metal complexes as therapeutic compounds has become more and more pronounced. These complexes offer a great diversity of uses in their medicinal applications. Electronic cigarettes (ECs) are an electronic nicotine delivery system that contain aerosol (ECR). The ligation behavior of prednisolone, which is a synthetic steroid that is used to treat allergic diseases and asthma arthritis, and its Zn (II) metal complex were studied and characterized based on elemental analysis, molar conductance, Fourier-transform infrared (FT-IR) spectra, electronic spectra, XRD, scanning electron microscopy (SEM), energy dispersive x-ray (EDX), and transmission electron microscopy (TEM). The FT-IR spectral data revealed that PRD acts as a mono-dentate ligand via oxygen atoms of the carbonyl group. Electronic and FT-IR data revealed that the PRD/Zn (II) metal complexes have square planer geometry. Artemisinin (ART) is the active main constituent of *Artemisia annua* extract, and it has been demonstrated to exert an excellent antimalarial effect. The experiment was performed on 40 male mice that were divided into the following 7 groups: Control, EC group, PRD/Zn, ART, EC plus PRD/Zn, EC plus ART, and PRD plus combination of PRD/Zn and ART. Serum CRP, IL-6, and antioxidants biomarkers were determined. Pulmonary tissue histology was evaluated. When in combination with Zn administration, PRD showed potent protective effects against pulmonary biochemical alterations induced by ECR and suppressed severe oxidative stress and pulmonary structure alterations. Additionally, PRD/Zn combined with ART prevented any stress on the pulmonary tissues via antioxidant regulation, reducing inflammatory markers CRP and Il-6 and improving antioxidant enzymatic levels more than either PRD or ART alone. Therefore, PRD/Zn combined with ART produced a synergistic effect against any sort of oxidative stress and also improved the histological structure of the lung tissues. These findings are of great importance for saving pulmonary function, especially during pandemic diseases, such as during the COVID-19 pandemic.

Keywords: electronic cigarette; prednisolone; metal complex; artemisinin

1. Introduction

Electronic cigarettes (also known as e-cigarettes, personal vaporizers, or vapes, and sometimes abbreviated to e-cigs) are electronic nicotine delivery systems (ENDSs). The E-cigarette is a battery-powered device that produces an aerosol that usually contains nicotine to be inhaled by heating a custom solution known as e-cigarette liquid (e-liquid) [1].

The first attempt to design a safer cigarette began after the high association between smoking and lung cancer was uncovered. As a result, E-cigarette popularity has been elevated tremendously over the past decades, especially due to advertisements and online marketing. Indeed, E-cigarettes (Figure 1) have been promoted as a smoking cessation method, a safer choice than smoking tobacco, and as a means to reduce smoking and to circumvent smoke free laws [2]. Additionally, E-cigarette components include propylene glycol (PG), glycerol/vegetable glycerin (VG), nicotine, flavors and sometimes colorings, which are food-grade or medical-grade. Although these materials are still not proven to be safe for inhalation, the use of food- and medical-grade ingredients has created a false perspective that using these e-cigarette is safe [2]. As such, E-cigarette popularity has increased tremendously over the past decade, especially due to frequent advertisements and online marketing.

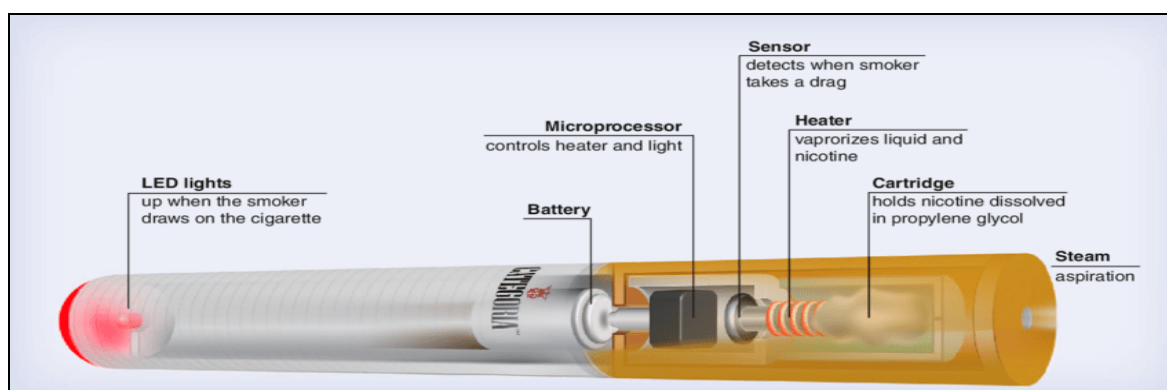


Figure 1. Structure of the e-cigarette (Caponnetto et al., 2012) [3].

The nature of the e-liquid materials changes after heating, leading to the formation of harmful compounds that are carcinogenic and neurotoxic, such as carbonyl compounds and volatile organic compounds (VOCs) [4]. Particulates and heavy metals are also found in the emitted aerosol [5].

By analyzing e-cigarette aerosol, formaldehyde, acetaldehyde, acetone, acrolein, and low amounts of propanol were found. The formation of formaldehyde and acrolein may result from heating glycerol. Furthermore, e-liquids with a greater glycerol percentage resulted in an increment of carbonyl compounds, such as acrolein. Different temperatures, flavors, and nicotine concentrations affect the amount of volatile evaporation [6].

The e-cigarette aerosol contains a high concentration of particulate nanometers. One puff of an e-cigarette results in the inhalation of about 2×10^6 nanoparticles cm^3 with a small size of less than 100 nm. Excessive exposure to nanoparticles can cause toxicity and degenerative diseases and may lead to brain damage [7].

The pulmonary system is the primary system to be exposed to aerosols from the e-cigarette, and most reports demonstrate the health effects that were associated with it. These health effects include headaches, dizziness, coughing, wheezing, asthma, and pneumonia [8].

The synthesis and study of inorganic complexes containing biologically important ligands is made easier because certain metal ions are active in many biological processes. Many synthesized mixed metal complexes have been reported to exhibit antimicrobial properties, and have been shown to be very potent against certain microorganisms [9].

Prednisolone (Figure 2) is a synthetic steroid that is used to treat a wide variety of chronic disorders, such as allergic diseases, asthma, and arthritis [10]. Prednisolone is

widely used in the management of a variety of diseases including severe asthma, and certain gastrointestinal, rheumatic, and hematological disorders [11]. However, a prednisolone therapeutic approach is also associated with some side effects, which may include an elevation in blood cholesterol, incidence of diabetes mellitus, elevated blood pressure and, finally, induction of weight gain [12,13]. Thus, we think that the complexation of prednisolone may reduce its prospective side effects, and may enhance its effectiveness in the treatment of various diseases.

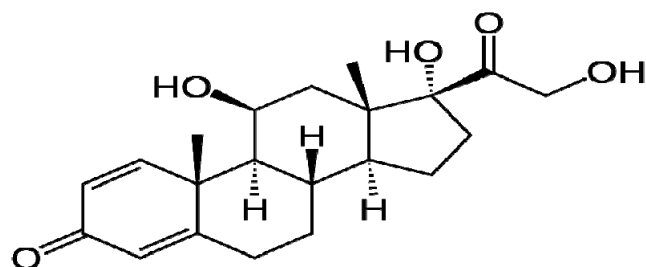


Figure 2. Chemical structure of prednisolone.

Synthetic glucocorticoids remain at the forefront of anti-inflammatory and immunosuppressive therapies. They are widely used to treat both acute and chronic inflammations, including rheumatoid arthritis and inflammatory diseases, as well as being used in immunosuppressive regimes following organ transplant. However, long-term use of oral glucocorticoids is associated with serious side effects, including an increased risk of cardiovascular diseases and metabolic diseases [14], and the discovery that many of the immunosuppressive actions of glucocorticoids are mediated by interference with the signaling by the key inflammatory transcriptional regulators [15]. Thus, carefully controlled doses, or novel complexes of metals with drugs, of the steroids are useful in suppressing the excessive and destructive immune response.

Artemisinin is the active main constituent of *Artemisia annua* extract, a plant used in traditional Chinese herbal remedies. Artemisinin is an effective constituent extracted from traditional Chinese medicine *Artemisia annua* L. Its chemical structure, which possesses a peroxide bridge, has been demonstrated to exert an excellent antimalarial effect [16]. In the presence of heme or free iron, the production of ROS (reactive oxygen species) and free radicals can directly poison the parasites [17].

Lopes et al. [18] synthesized and characterized new Zn (II) complexes with a cisplatin drug, and evaluated in vitro anti-proliferative activity, and their toxicological safety, using an alternative model (*Artemia salina* L.), as well as a BALB/c mouse model. They indicated that Zn (II) complexes with cisplatin might be a promising source of new metal-based antitumor agents. The complexes have been demonstrated to be safe for BALB/c mice when orally administered at the doses tested.

The prednisolone complexity with Zn (II) was investigated using FT-IR, molar conductance measurements, and magnetic moment testing. The spectroscopic results suggested structures for prepared prednisolone/Zn complexity. The chemical structure of prednisolone complexity was elucidated by FT-IR, XRD, SEM, and TEM. The aim of this work is the synthesis of novel prednisolone/Zn complexity, and to evaluate its effectiveness either alone or in combination with artemisinin in alleviating pulmonary dysfunction induced by excessive e-cigarette administration as a mimic of severe pulmonary inflammation and severe oxidative stress, such as happened during the COVID-19 pandemic.

2. Materials and Methods

2.1. Materials and Instrumentations

Prednisolone (PRD) (Figure 2) and ZnCl₂ used were purchased from the Aldrich Chemical Company, Burlington, MA, USA, which are of analytically reagent grade, and used without further purification. The C and H elements were performed using Vario

EL Fab. CHNS, Cairo, Egypt. The FT-IR spectrum of the zinc prednisolone complex was performed on a Bruker infrared spectrophotometer (Billerica, MA, USA) within the range of 400–4000 cm^{-1} . The molar conductance of 10^{-3} M solutions in DMSO solvent was measured at room temperature with freshly prepared solutions, using a HACH conductivity meter model. The electronic spectrum was scanned in situ DMSO within the 200–800 nm range using a Unicam UV/Vis spectrometer (Antwerpen, Belgium). The effective magnetic moment (μ_{eff}) of the zinc complex was measured using Gouy's method with the help of a magnetic susceptibility balance from the Johnson Matthey and Sherwood model. The SEM images were obtained using a JEOL (Tokyo, Japan) Jem-1200 EX II Electron microscope at an acceleration voltage of 25 kV. The transmission electron microscopy images (TEM) were performed using JEOL 100s microscopy.

Prednisolone (PRD), as a powder supplied as a vial (1 g), was obtained from Sigma-Aldrich Co. (St. Louis, MO, USA).

Commercially available e-cigarette aerosol were purchased (Ripe Vapes, Camarillo, California, USA) (VCT) (30 mg/mL). Artemisinin was purchased from KAN Phytochemicals Pvt, Ltd., Haryana, India). It was standardized to contain a minimum of 99% artemisinin (ART).

2.2. Synthesis of Zn (II) Complex

The $[\text{Zn}(\text{PRD})(\text{Cl})_2] \cdot \text{H}_2\text{O}$ complex was prepared from ZnCl_2 and (PRD) as explained below. Then, 20 mL of ZnCl_2 (1 mmol) in an aqueous solution, was added to a methanol solution (25 mL) of prednisolone (2 mmol). This was stirred and heated at 70 °C for 3 h. The pH of the solution mixture was adjusted between 8–9 using 1M NH_4OH , and then the complex was precipitated. Filtration was employed for the precipitate, and washing was performed using methanol. The precipitate was dried under vacuum in a desiccator using CaCl_2 . This resulted in a solid brownish yellow product with a (1:2) (Zn: PRD) molar proportion.

Analysis of the $\text{ZnC}_{21}\text{H}_{30}\text{O}_6\text{Cl}_2$, (487.38 g/mol) determined the following: %C 51.70 (51.62), %H 6.15 (6.11), %Cl 14.56 (14.53), and %Zn 13.41 (13.53). The C, H and Zn^{+2} analyses are convenient with the stoichiometry of Zn^{+2} : prednisolone is 1:1. The IR values in cm^{-1} using KBr tablets are as follows: 3250 $\nu(\text{OH})$, 1651 $\nu(\text{C}=\text{O})$, 1605 $\nu(\text{OH})$ water, 3278,3295 $\nu(\text{OH})$ water, 600–700 $\nu(\text{C}-\text{Cl})$, 520–506 $\nu(\text{Zn}-\text{O})$.

The chemical reaction scheme for the preparation of the zinc prednisolone complex can be summarized as follows: ZnCl_2 (1 mmol in 20 mL distilled water) + prednisolone (2 mmol in 25 mL methanol) \rightarrow stir and heat for 3 h \rightarrow add 1M NH_4OH \rightarrow adjust the pH (8–9) \rightarrow $[\text{Zn}(\text{PRD})(\text{Cl})_2] \cdot \text{H}_2\text{O} + \text{NH}_4\text{Cl}$.

2.3. E-Liquid Preparation (Aerosol)

Aerosol materials were purchased from an international online shop, and all were USP-grade. The e-liquid was prepared in the laboratory to ensure that its composition was controlled, which made it suit this experiment. The mixer was prepared with a 50/50 PG/VG ratio and a nicotine strength of 30 mg/mL. All measurements were scaled by weight (g), and all the calculations were performed using the Steam Engine online e-liquid calculation tool (version 5.1). (www.steam-engine.org, accessed on 2 March 2022).

2.4. Condensation of Aerosol

Treatment was prepared in the laboratory by compensating the e-cigarette aerosol to be injected into the eggs. First, the e-liquid was prepared manually in order to have control over the materials' percentages and to make sure of its authenticity. The device of evaporation was used with great care and in a clean and sterile manner, where the evaporator parts were disinfected with 70% ethanol after each use. The condensate was closely exposed to the animals of treatment in a closed box in order to ensure that the dosing came from inhalation only.

2.5. Experimental Animals

Experiments were conducted on 42 adult male mice (6 mice/group) weighing 30–35 g, in accordance with the guidance of the animal ethics for the handling and caring of the animals. Animal caring methods and experimental protocol were approved by the ethical committee of Zagazig University under approval number ZU-IACUC/2/F/61/2022, by following the guidelines of international animal care under this approval number. The experimental mice were kept in healthy conditions and provided with food and drink ad libitum.

2.6. Animal Model

2.6.1. Experimental Protocol

Male mice (body weight, 30–35 g) were divided into seven groups (six mice per group). Group I (the control group) was treated orally with physiological saline; group II were successively exposed to the prepared condensate of e-cigarette according to weight for 1/4 h for 30 days. Group III (the PRD group) received a single dose of PRD/Zn (II) ($5 \text{ mg}\cdot\text{kg}^{-1}$) [18], and was orally treated with ART (150 mg kg^{-1}) [19]; group IV was exposed to e-liquid evaporates followed by PRD/Zn; group V was exposed to e-liquid evaporates followed by ART; group VI was exposed to e-liquid evaporates followed by PRD/Zn and ART at the same dose described previously. The treatment timeline is shown in Figure 3.

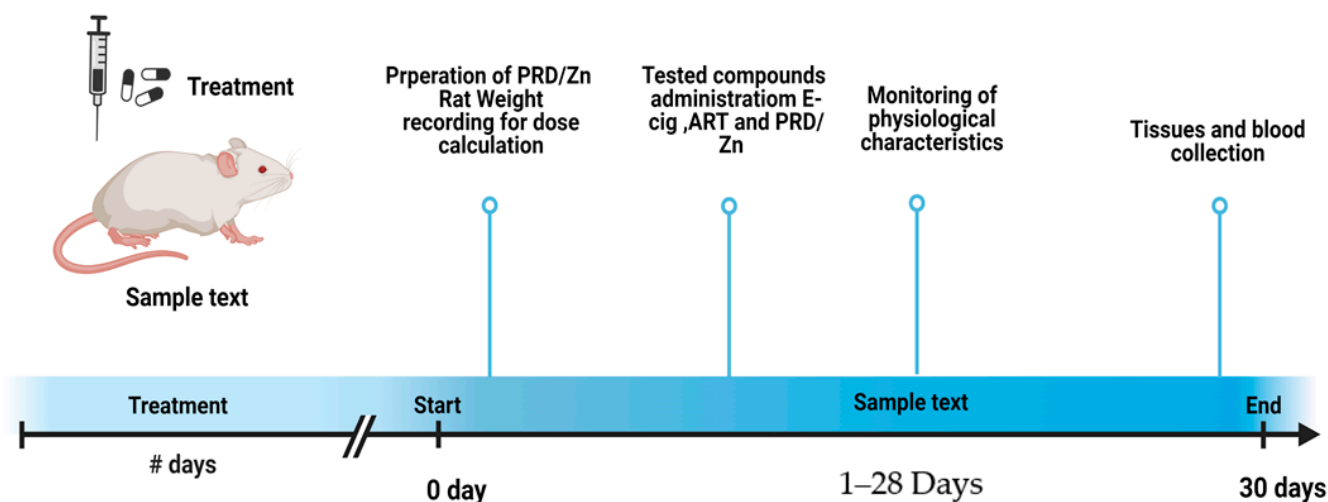


Figure 3. Timeline of the experiment.

2.6.2. Blood Samples

After the end of the experiment, blood samples were taken from the male mice eye plexus and divided into two parts. The first part was used to obtain plasma by the addition of samples in tubes with EDTA, and the second part was used to obtain serum by the addition of blood samples in tubes free of EDTA. The samples were centrifuged at 5000 rpm for 20 min.

2.6.3. Estimation of Inflammation Biomarkers

The C-reactive protein (CRP) and interleukins (Il-6) will be determined by Wener et al. [20] using the ELISA assay kit (SEA821, Aldrich Chemical Company).

2.6.4. Preparation of Pulmonary Tissue Homogenates for the Determination of Antioxidant Enzymes

A small lung portion was used to determine the oxidative stress markers. The pulmonary tissue was immersed in slightly basic phosphate buffer (pH 7.4), and then centrifuged. Then, we took the supernatant of the pulmonary tissue homogenates.

2.6.5. Determination of Oxidative Stress Biomarkers in Lung Tissues

The MDA level was determined according to Ohkawa et al. [21]. The SOD activity was determined according to Marklund and Marklund [22]. The CAT activity was evaluated according to Aebi [23]. The GRx was measured according to Couri and Abdel-Rahman [24]. Glutathione peroxidase (GPx) was evaluated according to Hafeman et al. [25].

2.6.6. Histological Changes

Small pulmonary tissue was immersed in 10% neutral buffered formalin for histological examination [26].

2.6.7. Antibacterial Activities

The antimicrobial activity of either PRD or PRD/Zn was determined. Antibacterial activity was tested in triplicate, and then the mean was calculated. In brief, 100 μL of the best bacteria was grown in 10 mL of fresh media until reaching an amount of approximately 108 cells/mL. Then, 100 μL of the microbial suspension was spread on to agar plates corresponding to the broth in which they were maintained. Isolated colonies of each organism that may play a pathogenic role were selected from the primary agar plates and tested for susceptibility by the disc diffusion method [27]. The Gram-positive bacteria *Bacillus subtilis* (Ehrenberg 23857TM) and *Streptococcus pneumoniae* (Klein) Chester (6303TM) and the Gram-negative bacteria *Escherichia coli* (BAA-2471TM) were incubated at 35–37 °C for 24–48 h. Afterwards, the inhibition zones' diameters were measured in millimeters [28,29]. Standard discs of tetracycline drug served as positive controls for the antimicrobial activity, and a filter disc impregnated with 10 μL solvent (dist. H₂O, DMSO) was used as a negative control. The agar used was the Mueller–Hinton agar, which was tested continuously in terms of its pH. Furthermore, the depth of the agar in the plates was considered in the disc diffusion method [30].

2.7. Statistical Analysis

Statistical analysis was performed using SPSS software version 27 and Open Epi version 2.3.1 [31]. Data were presented as mean \pm S.E. One-way ANOVA analysis, followed by a post hoc test, was used to analyze the data. A value of ($p < 0.05$) was accepted as statistically significant [32].

3. Results

3.1. Microanalytical and Molar Conductance Values

The synthesized zinc complex is a stable compound, insoluble in H₂O but with varying solubility in common organic solvents. The solid zinc complex is thermally stable, referring to a strong metal–ligand bond. The physical microanalytical data for the zinc complex is in agreement with its general formulation $[\text{Zn}(\text{PRD})_2(\text{Cl})_2]\cdot\text{H}_2\text{O}$. The molar conductance value of the complex in dimethyl sulfoxide (DMSO) at a 10^{-3} M concentration is $\Lambda_m = 31$ ($\Omega^{-1} \text{ mol}^{-1} \text{ cm}^{-1}$), indicating its non-electrolytic character [33–35], which refers to presence of Cl ions inside the sphere of coordination. The C and H and Zn analysis, as well as the molar conductance data, are accorded with general formula of $\text{Zn}\cdot(\text{PRD})_2\cdot(\text{Cl})_2\cdot\text{H}_2\text{O}$, formulated as $[\text{Zn}(\text{PRD})_2(\text{Cl})_2]\cdot\text{H}_2\text{O}$. The coordination modes of prednisolone toward the zinc (II) ion was explained using infrared, electronic spectra, magnetic moment, and molar conductance.

3.2. Infrared Spectra

The FT-IR spectrum for $[\text{Zn}(\text{PRD})_2(\text{Cl})_2]\cdot\text{H}_2\text{O}$ is shown in Figure 4. The IR for the prednisolone free ligand has an absorption band at 1651 cm^{-1} , which represents the carbonyl group, [36] while for the zinc complex this band is shifted to a lower wave number, confirming that C=O carbonyl is involved in the chelation process. For prednisolone free ligand, the stretching vibrational motion $\nu(\text{OH})$ for hydroxyl groups appeared at 3250 cm^{-1} , and for $[\text{Zn}(\text{PRD})_2(\text{Cl})_2]\cdot\text{H}_2\text{O}$ this band is located in the same position, confirming that

the OH group of prednisolone is not contributed in coordination with the Zn(II) ion. The infrared data for the Zn(II) complex shows a stretching vibration band at 3278 and 3295 cm^{-1} that are assigned to $\nu(\text{OH})$ of water molecules, while the band at 1605 cm^{-1} is assigned to hydroxyl group of H_2O of hydrated H_2O molecules, which supports the presence of H_2O outside the chelation sphere [37,38]. There are new bands that appear for the Zn(II) complex within wavenumbers 600–700 cm^{-1} , and these refer to the stretching vibration for the (Zn–Cl) bond [37,38].

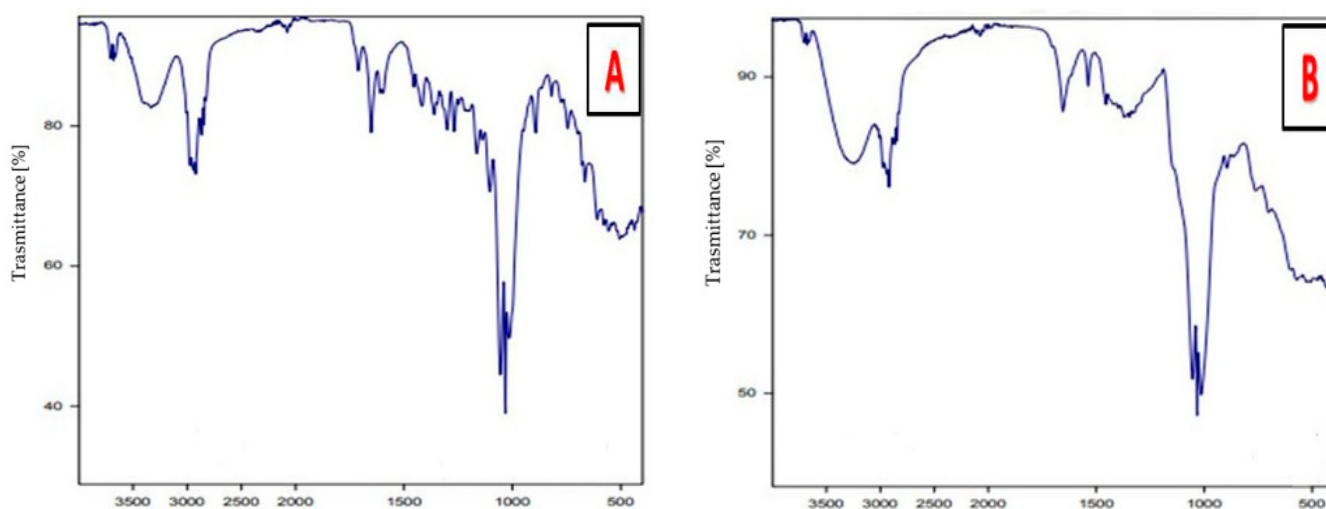


Figure 4. FT-IR of (A) PRD and (B) PRD/Zn.

The presence of new bands at 570–506 cm^{-1} that are assigned to the M–O stretching vibration range for the zinc complex (which absent in the free prednisolone ligand) provide evidence that the carbonyl group is bonded to the metal ion through the C=O group [36]. Therefore, prednisolone act as monodentate ligand and is coordinated toward the Zn (II) ion through the oxygen of the carbonyl group.

3.3. UV–Vis Spectra and Magnetic Data

The UV–Vis spectrum for free prednisolone showed absorbance bands in the UV region at 220 and 235 nm, which can be assigned to the $\pi \rightarrow \pi^*$ transition. For the $[\text{Zn}(\text{PRD})_2(\text{Cl})_2] \cdot \text{H}_2\text{O}$ complex, the electronic absorption spectra has three absorption bands at 225 nm, 245 nm, and 255 nm, respectively, due to the $\pi \rightarrow \pi^*$ electronic transitions (Table 1) [39]. The intensity of these bands in the prepared zinc complex is a convenient d^{10} configuration with tetrahedral geometry that could be possibly proposed for the Zn(II) complex and considered as diamagnetic, as shown in Figure 5.

Table 1. Electronic spectra and magnetic moments of free ligand prednisolone, and its zinc complex.

Sample	Electronic Bands/nm		Magnetic Moment	Geometry
	$\pi \rightarrow \pi^*$	$n \rightarrow \pi^*$		
Prednisolone	225 235	-	-	-
$[\text{Zn}(\text{PRD})_2(\text{Cl})_2] \cdot \text{H}_2\text{O}$	225 245 255	-	Diamagnetic	Square planar

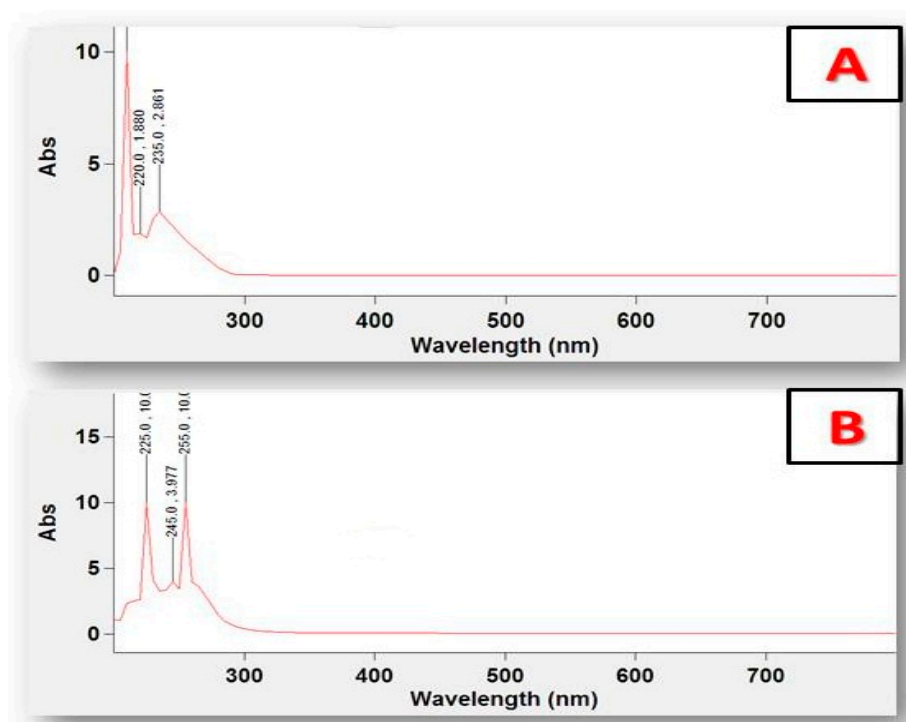


Figure 5. UV-Vis spectra of (A) PRD and (B) PRD/Zn.

3.4. X-ray Powder Diffraction

X-ray powder diffraction patterns were used to explain the crystallinity. X-ray powder diffraction patterns within a range of a diffraction angle of (2θ) 0 – 100° were used to investigate the nano structural form for the $[\text{Zn}(\text{PRD})_2(\text{Cl})_2]\cdot\text{H}_2\text{O}$ complex. The X-ray powder diffraction (XRD) patterns deduced that the zinc complex has an amorphous shape, as shown in Figure 4.

3.5. Scanning Electron Microscopy and Transmission Electron Microscopy Studies

The SEM images of the $[\text{Zn}(\text{PRD})_2(\text{Cl})_2]\cdot\text{H}_2\text{O}$ complex is shown in Figure 6. The investigated images for surface morphology having a lot of irregular shapes, and some have regular grains. The EdX confirmed the presence of Zn ions, as shown in Figure 7. The TEM images of the $[\text{Zn}(\text{PRD})_2(\text{Cl})_2]\cdot\text{H}_2\text{O}$ nanoparticles resulted from the reaction of zinc chloride salt with one mole of PRD and Zn, as shown in Figure 8. After the complete formation of new $[\text{Zn}(\text{PRD})_2(\text{Cl})_2]\cdot\text{H}_2\text{O}$, the size particle is in the range of 50 – 100 nm, with spherical black spots.

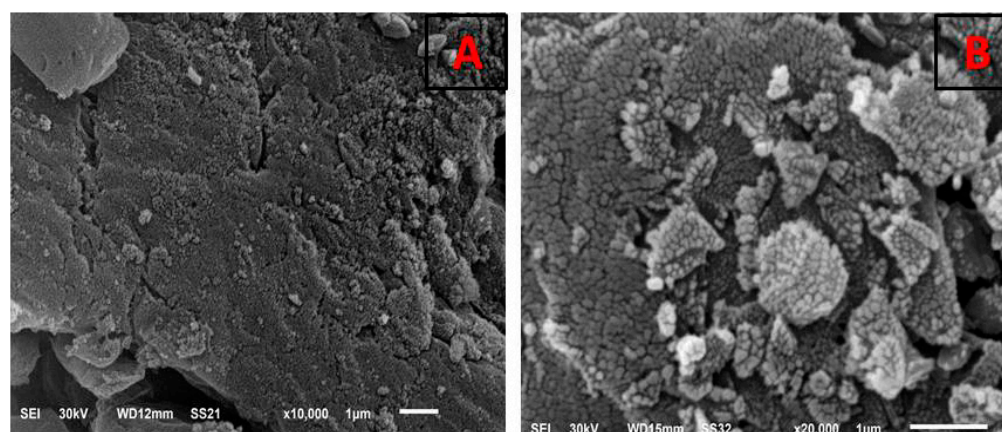


Figure 6. SEM of (A) PRD and (B) PRD/Zn.

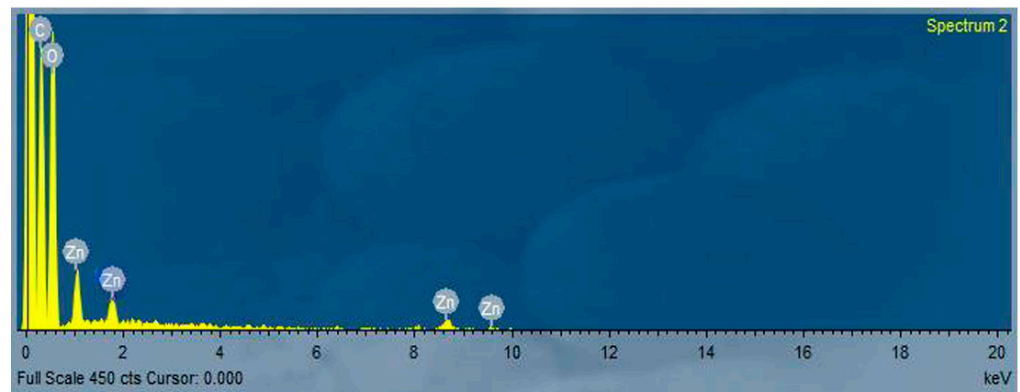


Figure 7. EDX of the PRD/Zn metal complex.

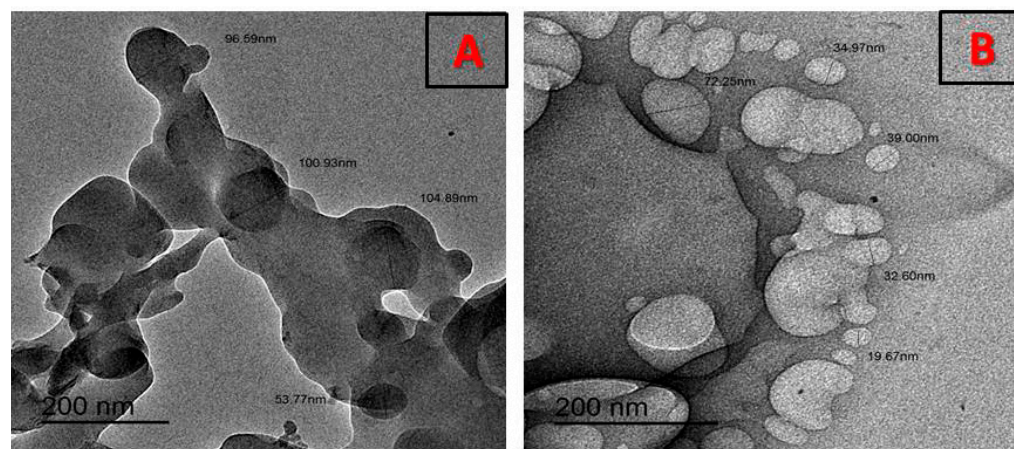


Figure 8. TEM of (A) PRD and (B) PRD/Zn.

3.6. Pulmonary Inflammation Markers

Both CRP and IL-6 were markedly elevated in the E-cig group in comparison with the normal control animals (Table 2). However, other treated groups with either the PRD/Zn complex or ART, or their combination, exhibited a significant decrease in both inflammatory markers after exposure to E-cig aerosol.

Table 2. Effects of E-cigs on inflammatory markers and beneficial effects of PRD/Zn and ART in male mice.

Parameters	Control	E-cig	PRD/Zn	ART	E-cig + PRD/Zn	E-cig + ART	E-cig + PRD/Zn+ ART
CRP (mg/L)	55.02 ± 4.25 ^c	187.25 ± 5.98 ^a	33.35 ± 4.25 ^d	28.25 ± 4.25 ^d	89.02 ± 4.25 ^b	92.98 ± 4.58 ^b	60.02 ± 5.21 ^c
IL-6 (pg/mL)	34.25 ± 4.02 ^d	220.03 ± 8.25 ^a	24.02 ± 4.55 ^e	20.36 ± 2.02 ^e	110.06 ± 4.25 ^b	125.03 ± 5.02 ^b	75.02 ± 4.02 ^c

Means within the same column (mean ± SE) with different letters are significant at $p \leq 0.05$ using Duncan's multiple range test, where the highest mean value has symbol ^a and ^{b–e} those decreasing in value are assigned alphabetically.

3.7. Oxidative Stress Enzymatic and Non-Enzymatic Biomarkers

Table 2 showed the alterations in oxidative/antioxidant enzymes in pulmonary tissues of control and treated male mice with PRD/Zn and/or ART. The MDA levels of E-cig treated animals were markedly elevated, with a decrease all the antioxidant enzymes (SOD, CAT, GRx, and GST). The combination of PRD/Zn caused MDA levels to decline significantly, and improved all the antioxidants more than treatment with E-cigs.

Continuous exposure to E-cig aerosol for successive 30 days resulted in a significant ($p < 0.0005$) decline in antioxidant enzymes (CAT, SOD, GRx, and GPx). Moreover, the E-cig aerosol showed a significant increment in MDA levels compared with the normal control group (Table 3).

Table 3. Effects of E-cigs on pulmonary antioxidant enzymes and beneficial effects of PRD/Zn and ART in lung homogenates of male mice.

Parameters	Normal	E-cig	PRD/Zn	ART			
	Control			E-cig + PRD/Zn	E-cig + ART	E-cig + PRD/Zn + ART	
CAT (U/g)	5.02 ± 0.58 ^b	1.02 ± 0.58 ^e	5.68 ± 1.02 ^{ab}	4.97 ± 0.58 ^c	4.82 ± 0.58 ^c	4.25 ± 0.67 ^d	4.99 ± 0.68 ^{cd}
SOD (U/g)	3.02 ± 0.87 ^c	0.58 ± 0.02 ^d	4.82 ± 0.58 ^a	4.01 ± 0.58 ^a	3.55 ± 0.87 ^c	3.05 ± 0.78 ^c	3.82 ± 0.25 ^{bc}
GRx (U/g)	4.98 ± 1.02 ^{ab}	1.25 ± 0.87 ^e	4.58 ± 1.58 ^{ab}	4.05 ± 1.69 ^b	2.58 ± 0.78 ^d	2.44 ± 0.61 ^d	3.77 ± 0.98 ^c
MDA (µg/mg)	3.01 ± 0.25 ^e	15.69 ± 0.58 ^a	4.25 ± 0.69 ^{de}	4.02 ± 1.25 ^{de}	8.02 ± 1.25 ^b	8.78 ± 2.25 ^b	6.02 ± 1.02 ^c
GPx (U/g)	8.87 ± 1.69 ^{ab}	2.058 ± 0.78 ^f	8.67 ± 1.58 ^{ab}	8.02 ± 2.02 ^b	4.02 ± 0.58 ^e	5.41 ± 1.66 ^{de}	7.02 ± 1.69 ^c

Means within the same column (mean ± SE) with different letters are significant at $p \leq 0.05$ using Duncan's multiple range test, where the highest mean value has symbol ^a and ^{b-e} those decreasing in value are assigned alphabetically.

3.8. Histological Examination

Figure 9 shows sections of pulmonary tissues displaying a normal structure in the control group, as well as abnormalities in the group successively exposed to the E-cig aerosol for 30 days. Meanwhile, there was great amelioration in groups treated with E-cig, combined with either PRD/Zn and/or ART and the best amelioration was recorded in the last group treated with a combination of PRD/Zn + ART after successive exposure to E-cigs for 30 days (Figure 9).

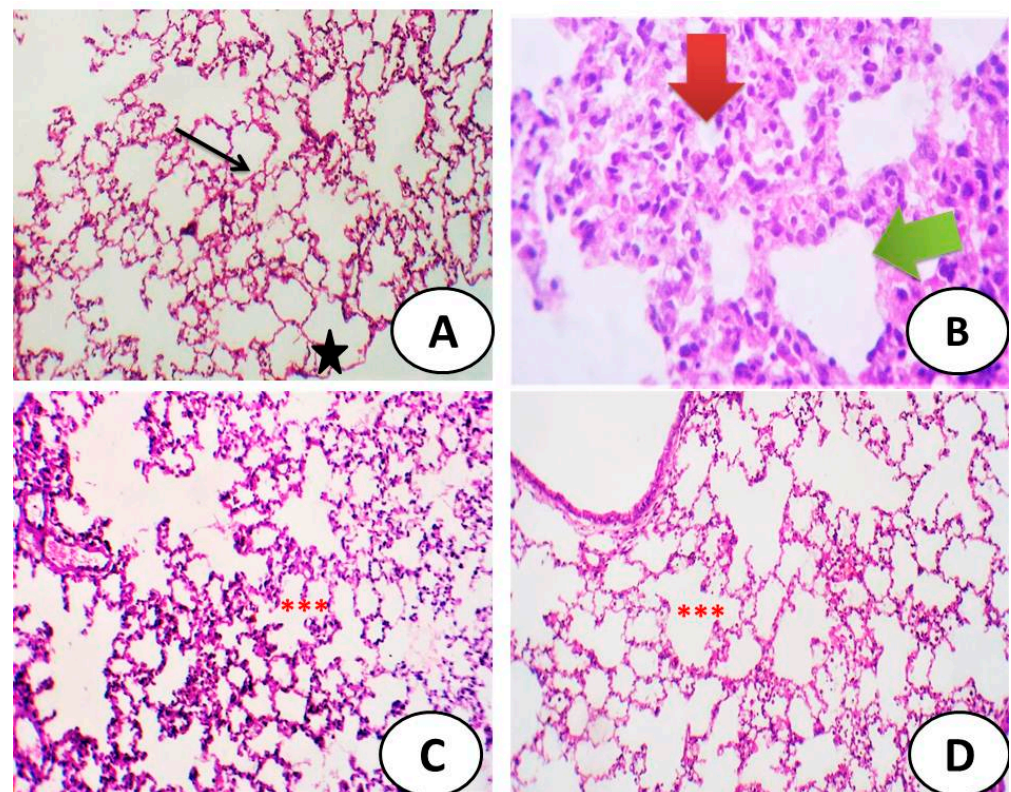


Figure 9. Cont.

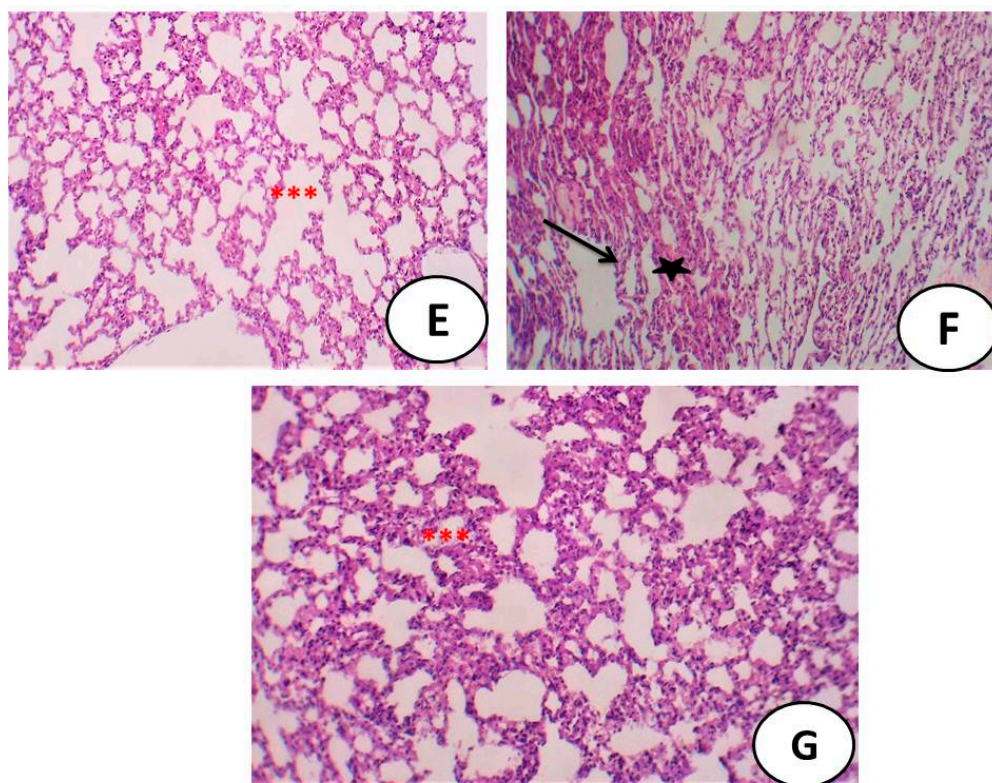


Figure 9. (A) Control group: photomicrograph of a cross-section of the pulmonary tissues, showing normal alveoli (black star) and interalveolar septa (arrow) (H&E \times 400). (B) Photomicrograph of the lungs of male mice after exposure to the aerosol of an E-cig, showing the loss of the normal architecture of the lung thickening of alveolar wall and marked interstitial inflammatory infiltrate (H&E \times 400). (C) Photomicrograph of the pulmonary tissues of PRD/Zn showing normal alveoli with interalveolar septa (***). (D) Photomicrograph of a cross-section of the pulmonary tissues of ART showing normal alveoli with interalveolar septa (***). (E) Cross-section of the lungs of male mice after the administration of the aerosol of an E-cig, followed by PRD/Zn, showing mild thickening of some alveoli (arrow), while other areas showed mild inflammatory infiltrate (star) (H&E \times 200). (F) Photomicrograph of the lungs of male mice after administration of the aerosol of an E-cig, followed by ART, showing mild thickening of some alveoli (arrow) while other areas showed mild inflammatory infiltrate (star) (H&E \times 200). (G) Photomicrograph of the lungs of male mice after the administration of the aerosol of an E-cig, followed by both PRD/Zn and ART, showing a high recovery of normal pulmonary tissues with partial subsiding of inflammation (***), with a mild thickness of alveoli (H&E \times 100).

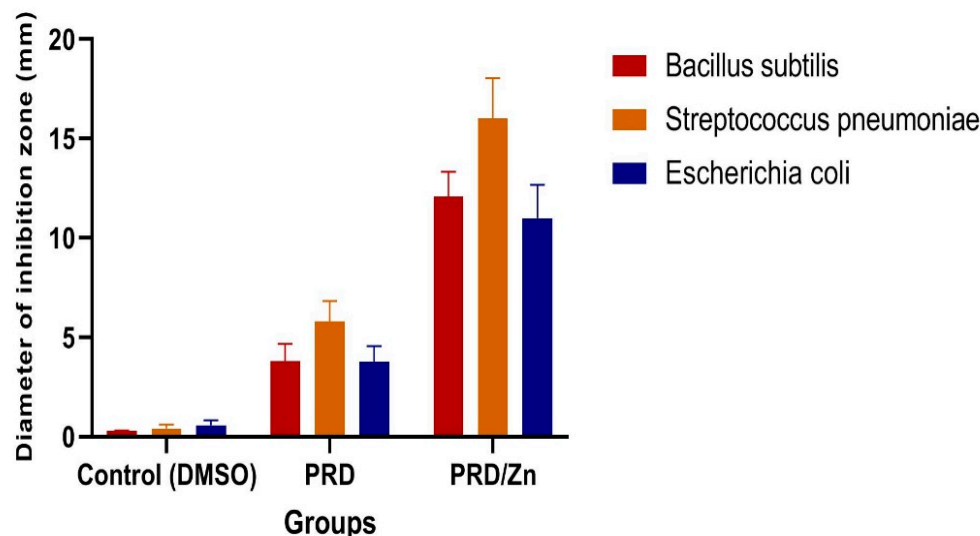
3.9. Antibacterial Activity Evaluation

Biological evaluations and antibacterial activity for the PRD/Zn complex were carried out against (*Bacillus subtilis* and *Streptococcus pneumoniae*) which are Gram-positive, and (*Escherichia coli*), which is Gram-negative bacteria. The results are shown in Table 4 and reported in Figure 10. The inhibition zones' diameter of the drug amikacin were found against Gram-positive bacteria and Gram-negative bacteria to be 36, 31, and 35 mm, respectively. Table 4 and Figure 10 showed that all the complexes were efficient, with a sufficient antimicrobial activity that exceeded PRD itself.

Table 4. Diameter of the inhibition zone (mm/mg sample) of the PRD and PRD/Zn metal complexes.

Sample	Inhibition Zone Diameter (mm/mg Sample)		
	<i>Bacillus subtilis</i> (G ⁺)	<i>Escherichia coli</i> (G ⁻)	<i>Streptococcus pneumoniae</i> (G ⁺)
Control (DMSO)	0.0 ± 0.0 ^c	0.01 ± 0.0 ^d	0.0 ± 0.0 ^d
PRD	3.80 ± 0.11 ^b	3.76 ± 0.31 ^c	5.8 ± 0.73 ^c
PRD/Zn	12 ± 0.62 ^a	10.98 ± 0.96 ^a	16 ± 0.21 ^a

Means within the same column (mean ± SE) carrying different letters are significant at $p \leq 0.05$, where the highest mean value has the symbol ^a and ^{b-d} those decreasing in value are assigned alphabetically.

**Figure 10.** Antibacterial activity of the PRD and PRD/Zn metal complexes.

4. Discussion

Previous studies showed that E-cigarette aerosols showed diverse health effects [40]. The main risk of using E-cigarettes, is their deleterious effects on pulmonary tissues and the induction of severe oxidative stress in different organs of the body. Thus we determined to use novel metal complex of PRD/ZN in combination with ART to alleviate the side effects of E-cigarettes and to elevate immune response and enhance pulmonary functions, to be an adjuvant therapy during pandemic diseases.

Recently, Sassano et al. [41] proved that the two primary ingredients found in e-cigarettes—propylene glycol and vegetable glycerin—are highly toxic to cells, and that the more ingredients in an e-liquid, the greater the toxicity. This confirmed the obtained results of the current study, which showed the high toxicity of e-cigarette aerosol on pulmonary tissues that was proved by histological examination that clarifies the loss of normal architecture of lung thickening of the alveolar wall, as well as marked interstitial inflammatory infiltrate. These findings, in addition to the elevation of the inflammatory markers CRP and IL-6, confirmed this concept greatly.

Confirming the current concept of the study about the risk of e-cigarette aerosol, previous studies confirmed that there is evidence of the chemical transformation of propylene, which is one of the ingredients of e-cigarettes, after vaping to relatively toxic compounds. This depend on flavor, and this confirmed the current finding via the presence of pulmonary toxicity induced after exposure to aerosol and, thus, there is an increment in e-cigarette toxicity after vaping.

The actual deposition of e-liquids that were vaped into the pulmonary tissues remains recently evaluated. However, the predicted E-cig aerosol deposition in the lungs is approximately 25% [42]. Therefore, if 1 mL of e-liquid is inhaled and, assuming a total volume airway surface of the e-liquids in the pulmonary tissues of approximately 3 mL, this would lead to 1/4 mL being deposited, suggesting that the dilution factor is about 1:12,

or equivalent to approximately 8%. It has been previously proven that e-liquids have a LC50 that is about 6% or perhaps less, and this would suggest that the liquids in e-cigarettes may reach biologically relevant levels in the pulmonary tissues. Additionally, it has been recently demonstrated that vaping significantly alters the secreted human airway's internal structures [43]. Thus, we are still discovering the relative e-cigarette toxicity of liquid constituents and their implications for the pulmonary airways.

Propylene glycol is a chemical that is the main constituent of E-cigarette liquid. Previous studies confirmed that PG can induce acute renal and neurotoxicity [44] and, thus, propylene glycol inhalation can cause both hepatic and renal toxicity [45]. These findings are in parallel with the current finding that previously showed that propylene glycol causes a disturbance of renal glucose transport [46,47].

Corticosteroids are used widely for the prevention of bronchopulmonary dysplasia. Proposed mechanisms include the promotion of antioxidant lung enzymes, the inhibition of inflammatory cell infiltration, and the reduction of the severe pulmonary edema [48]. Prednisolone is an attractive choice for this patient population given its successful use in pulmonary disease states, such as asthma [49].

The majority of controlled trials focus on using dexamethasone or hydrocortisone. Despite this, many patients still develop severe pulmonary diseases, especially during pandemic diseases, such as COVID-19, and there is limited evidence to inform on the risks and benefits of the use of corticosteroids with established bronchopulmonary dysplasia [50]. Thus, the main goal of the current study was to test the effect of a novel complex of PRD/Zn on pulmonary functions and antioxidant enzymes with beneficial effects on the lung tissues, and the enhancement of the immune system, especially during pandemic diseases, such as the COVID-19 pandemic.

Hryniewicka et al. [51] demonstrated that some of the new steroid salts exhibited high antifungal activities, and that these new compounds could be potentially useful in inhibiting agents against pathogenic fungi. This confirmed the high antibacterial activities of the novel synthesized PRD/Zn complex.

Artemisinin, a natural product, has received considerable attention in the last few years as a potent antimalarial drug. Xia et al. [52] demonstrated that animal studies showed that artesunate can increase renal blood flow, while in a clinical study, liver function, kidney function, and routine blood tests remained normal in most patients treated with artesunate [53], and this confirmed the obtained results that proved ART beneficial effects without incidence of organ toxicity.

Ahmed-Laloui et al. [54] tested the antioxidant capacities of three different Artemisia species and assessed their chemical structure using HPLC. They demonstrated that there was a remarkable antioxidant capacity found in all artemisia methanolic extracts analyzed, and this confirmed the great antioxidant capacities of ART against oxidative injury induced by e-cigarette aerosol and also improved the histological structure of the lung and reduced oxidative stress greatly.

5. Conclusions

The current study demonstrated that pulmonary tissues were affected by E-cigarette administration, and that pulmonary tissues were greatly improved after PRD/Zn complex administration with ART, which ameliorated inflammation markers and has contributed to an improvement in the pulmonary functions than was observed when using of E-cigarette. Our results confirmed that the PRD/Zn complex in combination with ART were effective and safe for the treatment of pathological alterations in the lung tissues and any sort of oxidative injury with more antioxidant capacity. These novel results open a new avenue to develop new therapeutic combination strategies for saving the health of the pulmonary tissues or even the prevention of any respiratory complications, such as during the COVID-19 pandemic and declined inflammatory markers that can reduce the need for mechanical ventilation in pandemic respiratory diseases.

Author Contributions: Conceptualization, R.Z.H., R.E.A., F.S.A., N.M.A.-B., B.A.-B., M.A.A.-H., G.S.A., N.A.A.-S., F.S.A., A.A.A.-T., S.M.E.-M. and E.H.A.-T.; methodology, R.Z.H., R.E.A., F.S.A., M.A.A.-H., G.S.A., N.A.A.-S., N.M.A.-B., B.A.-B., A.A.A.-T., S.M.E.-M. and E.H.A.-T.; software, R.Z.H., R.E.A., M.A.A.-H., G.S.A., N.A.A.-S., F.S.A., A.A.A.-T., S.M.E.-M. and E.H.A.-T.; validation, R.Z.H., R.E.A., M.A.A.-H., G.S.A., N.A.A.-S., A.A.A.-T., N.M.A.-B., B.A.-B., S.M.E.-M. and E.H.A.-T.; formal analysis, R.Z.H. and S.M.E.-M.; investigation, R.Z.H., R.E.A., M.A.A.-H., F.S.A., N.M.A.-B., B.A.-B., G.S.A., N.A.A.-S., A.A.A.-T., S.M.E.-M. and E.H.A.-T.; data curation, R.Z.H., R.E.A., M.A.A.-H., G.S.A., N.A.A.-S., A.A.A.-T., S.M.E.-M. and E.H.A.-T.; writing—original draft preparation, R.Z.H., R.E.A., F.S.A., M.A.A.-H., G.S.A., N.M.A.-B., B.A.-B., N.A.A.-S., A.A.A.-T., S.M.E.-M., F.S.A. and E.H.A.-T.; writing—review and editing, R.Z.H., R.E.A., M.A.A.-H., G.S.A., N.A.A.-S., A.A.A.-T., S.M.E.-M. and E.H.A.-T.; visualization, R.Z.H., R.E.A., N.M.A.-B., B.A.-B., M.A.A.-H., G.S.A., N.A.A.-S., A.A.A.-T., S.M.E.-M. and E.H.A.-T.; supervision, F.S.A., R.Z.H., S.M.E.-M. and E.H.A.-T.; project administration, R.Z.H., R.E.A., M.A.A.-H., G.S.A., N.M.A.-B., B.A.-B., N.A.A.-S., A.A.A.-T., S.M.E.-M. and E.H.A.-T.; funding acquisition, R.Z.H., S.M.E.-M. and E.H.A.-T. All authors have read and agreed to the published version of the manuscript.

Funding: This research received no external funding.

Institutional Review Board Statement: Animal caring methods and experimental protocol were approved by ethical committee of Zagazig university under approval number: ZU-IACUC/2/F/61/2022 by following the guidelines of the international animal care under this approval number.

Informed Consent Statement: Animal caring methods and experimental protocol were approved by ethical committee of Zagazig university under approval number: ZU-IACUC/2/F/61/2022 by following the guidelines of the international animal care under this approval number.

Data Availability Statement: All the Data are available within the text.

Acknowledgments: Authors acknowledge Taif University Researchers Supporting number (TURSP-2020/21), Taif University, Taif, Saudi Arabia.

Conflicts of Interest: The authors declare no conflict of interest.

References

1. Goniewicz, M.L.; Knysak, J.; Gawron, M.; Kosmider, L.; Sobczak, A.; Kurek, J.; Benowitz, N. Levels of selected carcinogens and toxicants in vapour from electronic cigarettes. *Tob. Control* **2014**, *23*, 133–139. [[CrossRef](#)] [[PubMed](#)]
2. Grana, R.A.; Ling, P.M. “Smoking revolution”: A content analysis of electronic cigarette retail websites. *Am. J. Prev. Med.* **2014**, *46*, 395–403. [[CrossRef](#)] [[PubMed](#)]
3. Caponnetto, P.; Campagna, D.; Papale, G.; Russo, C.; Polosa, R. The emerging phenomenon of electronic cigarettes. *Expert Rev. Respir. Med.* **2012**, *6*, 63–74. [[CrossRef](#)] [[PubMed](#)]
4. Lee, S.M.; Le Bouf, R.F.; Son, Y.; Koutrakis, P.; Christiani, D.C. Nicotine, aerosol particles, carbonyls and volatile organic compounds in tobacco and menthol-flavored e-cigarettes. *Environ. Health* **2017**, *16*, 42. [[CrossRef](#)]
5. Herrington, J.S.; Myers, C. Electronic cigarette solutions and resultant aerosol profiles. *J. Chromatogr. A* **2015**, *1418*, 192–199. [[CrossRef](#)]
6. Yi, L.; Yichen, W.; Liqiao, L.; Yuening, G.; Ege, Ç.; Yifang, Z.; Aydogan, O. Dynamic Imaging and Characterization of Volatile Aerosols in E-Cigarette Emissions Using Deep Learning-Based Holographic Microscopy. *ACS Sens.* **2021**, *6*, 2403–2410.
7. Mikheev, V.B.; Ivanov, A.; Lucas, E.A.; South, P.L.; Colijn, H.O.; Clark, P.I. Aerosol size distribution measurement of electronic cigarette emissions using combined differential mobility and inertial impaction methods: Smoking machine and puff topography influence. *Aerosol. Sci. Technol.* **2018**, *52*, 1233–1248. [[CrossRef](#)]
8. Hua, M.; Sadah, S.; Hristidis, V.; Talbot, P. Health effects associated with Electronic cigarette use: Automated Mining of online forums. *J. Med. Internet Res.* **2020**, *22*, e15684. [[CrossRef](#)]
9. Olagboye, S.A.; Adekeye, D.K.; Akinwunmi, O.A. Antimicrobial activities of novel synthesized Cu (II) and Co (II) mixed ligand complexes of prednisolone and paracetamol. *Int. J. Sci. Eng. Res.* **2020**, *10*, 651–662.
10. Osowole, A.A.; Wakil, A.S.; Alao, K.O. Synthesis, characterization and antimicrobial activity orsome mixed Trimethoprim-sulfamethoxazole metal drug complexes. *World Appl. Sci. J.* **2015**, *33*, 336–342.
11. Raman, N.; Sobha, S. Synthesis, characterization and antimicrobial screening of isatin—Based polypyridyl mixed ligand Cu (II) and Zn (II) complexes. *J. Serb. Chem. Soc.* **2010**, *17*, 733–788. [[CrossRef](#)]
12. Vogt, M.; Derendorf, H.; Kramer, J.; Junginger, H.E.; Midha, K.K.; Shah, V.P.; Stavchansky, S.; Dressman, J.B.; Barends, D.M. Biowaiver monographs for immediate release solid oral dosage forms: Prednisolone. *J. Pharm. Sci.* **2006**, *96*, 27–37. [[CrossRef](#)] [[PubMed](#)]

13. Pickup, M.E.; Lowe, J.R.; Leatham, P.A.; Rhind, V.M.; Wright, V.; Downie, W.W. Dose dependent pharmacokinetics of prednisolone. *Eur. J. Clin. Pharmacol.* **1977**, *12*, 213–219. [CrossRef] [PubMed]
14. Coutinho, A.E.; Chapman, K.E. The anti-inflammatory and immunosuppressive effects of glucocorticoids, recent developments and mechanistic insights. *Mol. Cell Endocrinol.* **2011**, *335*, 2–13. [CrossRef]
15. Wei, L.; MacDonald, T.M.; Walker, B.R. Taking glucocorticoids by prescription is associated with subsequent cardiovascular disease. *Ann. Intern. Med.* **2004**, *141*, 764–770. [CrossRef]
16. Xia, M.; Liu, D.; Liu, Y.; Liu, H. The Therapeutic Effect of Artemisinin and Its Derivatives in Kidney Disease. *Front. Pharmacol.* **2020**, *11*, 380. [CrossRef]
17. An, J.; Minie, M.; Sasaki, T.; Woodward, J.J.; Elkon, K.B. Antimalarial Drugs as Immune Modulators: New Mechanisms for Old Drugs. *Annu. Rev. Med.* **2017**, *68*, 317–330. [CrossRef]
18. Lopes, E.d.; de Oliveira, C.G.; da Silva, P.B.; Eismann, C.E.; Suárez, C.A.; Menegário, A.A.; Leite, C.Q.F.; Deflon, V.M.; Pavan, F.R. Novel Zinc(II) Complexes [Zn(atc-Et)₂] and [Zn(atc-Ph)₂]: In Vitro and in Vivo Antiproliferative Studies. *Int. J. Mol. Sci.* **2016**, *17*, 781. [CrossRef]
19. Wu, X.; Wang, X.; Zhang, W.; Shi, X.; An, P.; Sun, W.; Wang, Z. Therapeutic effect of artemisinin on lupus nephritis mice and its mechanisms. *Acta Biochim. Biophys. Sin.* **2010**, *42*, 916–923. [CrossRef]
20. Wener, M.H.; Daum, P.R.; McQuillin, G.M. The influence of age, sex, and race on the upper reference limit of serum C-reactive protein concentration. *J. Rheumatol.* **2000**, *27*, 2351–2359.
21. Ohkawa, H.; Ohishi, N.; Yagi, K. Assay for lipid peroxides in animal tissues by thiobarbituric acid reaction. *Anal. Biochem.* **1979**, *95*, 351–358. [CrossRef]
22. Marklund, S.; Marklund, G. Involvement of the superoxide anion radical in the autoxidation of pyrogallol and a convenient assay for superoxide dismutase. *Eur. J. Biochem.* **1974**, *47*, 469–474. [CrossRef] [PubMed]
23. Aebi, H.E. Catalase. In *Methods of Enzymatic Analysis*; Elsevier: Amsterdam, The Netherlands, 1983.
24. Couri, D.; Abdel-Rahman, M.S. Effect of chlorine dioxide and metabolites on glutathione dependent system in rat, mouse and chicken blood. *J. Environ. Pathol. Toxicol.* **1979**, *3*, 451–460.
25. Hafeman, D.G.; Sunde, R.A.; Hoekstra, W.G. Effect of dietary selenium on erythrocyte and liver glutathione peroxidase in the rat. *J. Nutr.* **1974**, *104*, 580–587. [CrossRef] [PubMed]
26. Hayat, M. *Basic Techniques for Transmission Electron Microscopy*; Elsevier: Amsterdam, The Netherlands, 2012.
27. Pfaller, M.A.; Burmeister, L.; Bartlett, M.A.; Rinaldi, M.G. Multicenter evaluation of four methods of yeast inoculum preparation. *J. Clin. Microbiol.* **1988**, *26*, 1437–1441. [CrossRef] [PubMed]
28. El-Megharbel, S.M.; Al-Thubaiti, E.H.; Qahl, S.H.; Al-Eisa, R.A.; Hamza, R.Z. Synthesis and Spectroscopic Characterization of Dapagliflozin/Zn (II), Cr (III) and Se (IV) Novel Complexes That Ameliorate Hepatic Damage, Hyperglycemia and Oxidative Injury Induced by Streptozotocin-Induced Diabetic Male Rats and Their Antibacterial Activity. *Crystals* **2022**, *12*, 304.
29. M7-A3; Methods for Dilution Antimicrobial Susceptibility Tests for Bacteria That Grow Aerobically. National Committee for Clinical Laboratory Standards conference: Villanova, PA, USA, 1993.
30. Liebowitz, L.D.; Ashbee, H.R.; Evans, E.G.V.; Chong, Y.; Mallatova, N.; Zaidi, M.; Gibbs, D. A two year global evaluation of the susceptibility of *Candida* species to fluconazole by disk diffusion. *Diagn. Microbiol. Infect. Dis.* **2001**, *40*, 27–33. [CrossRef]
31. IBM. IBM SPSS Statistics for Windows, Version 27. Armonk, NY: IBM Corp. 2020. Available online: <http://www-01.ibm.com/support/docview.wss?uid=swg27049428> (accessed on 2 March 2022).
32. Dean, A.; Sullivan, K.; Soe, M. OpenEpi: Open Source Epidemiologic Statistics for Public Health. 2013. Available online: <https://www.OpenEpi.com> (accessed on 2 March 2022).
33. El-Megharbel, S.M.; Hamza, R.Z. Synthesis, spectroscopic characterizations, conductometric titration and investigation of potent antioxidant activities of gallic acid complexes with Ca (II), Cu (II), Zn(III), Cr(III) and Se (IV) metal ions. *J. Mol. Liq.* **2022**, *358*, 119196. [CrossRef]
34. El-Megharbel, S.M.; Al-Baqami, N.M.; Al-Thubaiti, E.H.; Qahl, S.H.; Albogami, B.; Hamza, R.Z. Antidiabetic Drug Sitagliptin with Divalent Transition Metals Manganese and Cobalt: Synthesis, Structure, Characterization Antibacterial and Antioxidative Effects in Liver Tissues. *Curr. Issues Mol. Biol.* **2022**, *44*, 1810–1827. [CrossRef]
35. El-Megharbel, S.M.; Qahl, S.H.; Alaryani, F.S.; Hamza, R.Z. Synthesis, Spectroscopic Studies for Five New Mg (II), Fe (III), Cu (II), Zn (II) and Se (IV) Ceftriaxone Antibiotic Drug Complexes and Their Possible Hepatoprotective and Antioxidant Capacities. *Antibiotics* **2022**, *11*, 547. [CrossRef]
36. Cotton, F.A.; Wilkinson, C.W. *Advanced Inorganic Chemistry*, 3rd ed.; Interscience Publisher: New York, NY, USA, 1972.
37. Nakamoto, K. *Infrared Spectra of Inorganic and Coordination Compounds*, 2nd ed.; Wiley Interscience; John Wiley & Sons: New York, NY, USA, 1970.
38. Bellamy, L.J. *The Infrared Spectra of Complex Molecules*; Chapman and Hall: London, UK, 1975.
39. Bukhari, I.H.; Arif, M.; Akbar, J.; Khan, A.H. Preparation, Characterization and Biological Evaluation of Schiff base and Transition Metal Complexes with Cephredine. *Pak. J. Biol. Sci.* **2005**, *84*, 614–617.
40. Gulee, M.; Songur, A.; Sahin, S.; Ozen, O.A.; Sarsilmaz, M.; Akyol, O. Antioxidant enzyme activities and lipid peroxidation products in heart tissue of subacute and subchronic formaldehyde-exposed rats: A preliminary study. *Toxicol. Ind. Health* **2006**, *22*, 117–124.

41. Sassano, M.F.; Davis, E.S.; Keating, J.E.; Zorn, B.T.; Kochar, T.K.; Wolfgang, M.C.; Glish, G.L.; Tarran, R. Evaluation of e-liquid toxicity using an opensource high-throughput screening assay. *PLoS Biol.* **2018**, *16*, e2003904. [[CrossRef](#)] [[PubMed](#)]
42. Sosnowski, T.R.; Kramek-Romanowska, K. Predicted Deposition of E-Cigarette Aerosol in the Human Lungs. *J. Aerosol. Med. Pulm. Drug Deliv.* **2016**, *29*, 299–309. [[CrossRef](#)] [[PubMed](#)]
43. Reidel, B.; Radicioni, G.; Clapp, P.W.; Ford, A.A.; Abdelwahab, S.; Rebuli, M.E.; Haridass, P.; Alexis, N.E.; Jaspers, I.; Kesimer, M. E-Cigarette Use Causes a Unique Innate Immune Response in the Lung Involving Increased Neutrophilic Activation and Altered Mucin Secretion. *Am. J. Respir. Crit. Care Med.* **2018**, *197*, 492–501. [[CrossRef](#)] [[PubMed](#)]
44. Doi, A.M.; Roycroft, J.H.; Herbert, R.A.; Haseman, J.K.; Hailey, J.R.; Chou, B.J.; Dill, J.A.; Grumbein, S.L.; Miller, R.A.; Renne, R.A.; et al. Inhalation toxicology and carcinogenesis studies of propylene glycol mono-t-butyl ether in rats and mice. *Toxicology* **2004**, *199*, 1–22. [[CrossRef](#)]
45. Blake, D.A.; Whikehart, D.R.; Yu, H.; Vogel, T.; Roberts, D.D. Common cryopreservation media deplete corneal endothelial cell plasma membrane Na⁺,K⁺ ATPase activity. *Curr. Eye Res.* **1996**, *15*, 263–271. [[CrossRef](#)]
46. Morshed, K.M.; Jain, S.K.; McMartin, K.E. Acute toxicity of propylene glycol: An assessment using cultured proximal tubule cells of human origin. *Fundam. Appl. Toxicol.* **1994**, *23*, 38–43. [[CrossRef](#)]
47. Galbraith, D.A. Diacetyl and occupational bronchiolitis obliterans: Comments on Rose, CS: Early detection, clinical diagnosis and management of lung disease from exposure to diacetyl. *Toxicology* **2017**, *392*, 155–157. [[CrossRef](#)]
48. Breland, A.; Soule, E.; Lopez, A.; Ramoa, C.; El-Hellani, A.; Eissenberg, T. Electronic cigarettes: What are they and what do they do? *Ann. N. Y. Acad. Sci.* **2017**, *1394*, 5–30. [[CrossRef](#)]
49. Schroeder, M.J.; Hoffman, A.C. Electronic cigarettes and nicotine clinical pharmacology. *Tob. Control.* **2014**, *23*, ii30–ii35. [[CrossRef](#)] [[PubMed](#)]
50. Caren, L.; Zachary, V.; Brandy, Z.; Rakesh, R.; Christopher, M. Respiratory effects of prolonged prednisolone use in infants with evolving and established Bronchopulmonary dysplasia. *Early Hum. Dev.* **2021**, *156*, 105344.
51. Hryniewicka, A.; Malinowska, M.; Hauschild, T.; Morzycki, J.W. Synthesis and antimicrobial properties of steroid-based imidazolium salts. *J. Steroid Biochem. Mol. Biol.* **2019**, *189*, 65–72. [[CrossRef](#)]
52. Xia, M.; Liu, D.; Tang, X.; Liu, Y.; Liu, H.; Liu, Y.; Chen, G.; Liu, H. Dihydroartemisinin inhibits the proliferation of IgAN mesangial cells through the mTOR signaling pathway. *Int. Immunopharmacol.* **2020**, *80*, 106125. [[CrossRef](#)]
53. Von Hagens, C.; Walter-Sack, I.; Goeckenjan, M.; Osburg, J.; Storch-Hagenlocher, B.; Sertel, S.; Elsässer, M.; Remppis, B.A.; Edler, L.; Munzinger, J.; et al. Prospective open uncontrolled phase I study to define a well-tolerated dose of oral artesunate as add-on therapy in patients with metastatic breast cancer (ARTIC M33/2). *Breast Cancer Res. Treat.* **2017**, *164*, 359–369. [[CrossRef](#)] [[PubMed](#)]
54. Ahmed-Laloui, H.; Zaak, H.; Rahmani, A.; Kashi, I.; Chemat, S.; Miara, M.D.; Cherb, N.; Derdour, M. Assessment of artemisinin and antioxidant activities of three wild *Artemisia* species of Algeria. *Nat. Prod. Res.* **2022**, *9*, 1–9. [[CrossRef](#)] [[PubMed](#)]